J Neurophysiol 108: 658–671, 2012.
First published April 11, 2012; doi:10.1152/jn.00708.2011.

β-Adrenergic modulation of spontaneous spatiotemporal activity patterns and synchrony in hyperexcitable hippocampal circuits

Anupam Hazra,[1] Robert Rosenbaum,[2] Bernhard Bodmann,[2] Siyuan Cao,[3,4] Krešimir Josić,[1,2] and Jokūbas Žiburkus[1]

[1]*Department of Biology and Biochemistry, University of Houston, Houston, Texas;* [2]*Department of Mathematics, University of Houston, Houston, Texas;* [3]*Department of Earth and Atmospheric Sciences, University of Houston, Houston, Texas; and* [4]*State Key Laboratory of Petroleum Resource and Prospecting, China University of Petroleum, Beijing, China*

Submitted 28 July 2011; accepted in final form 7 April 2012

Hazra A, Rosenbaum R, Bodmann B, Cao S, Josić K, Žiburkus J. β-Adrenergic modulation of spontaneous spatiotemporal activity patterns and synchrony in hyperexcitable hippocampal circuits. *J Neurophysiol* 108: 658–671, 2012. First published April 11, 2012; doi:10.1152/jn.00708.2011.—A description of healthy and pathological brain dynamics requires an understanding of spatiotemporal patterns of neural activity and characteristics of its propagation between interconnected circuits. However, the structure and modulation of the neural activation maps underlying these patterns and their propagation remain elusive. We investigated effects of β-adrenergic receptor (β-AR) stimulation on the spatiotemporal characteristics of emergent activity in rat hippocampal circuits. Synchronized epileptiform-like activity, such as interictal bursts (IBs) and ictal-like events (ILEs), were evoked by 4-aminopyridine (4-AP), and their dynamics were studied using a combination of electrophysiology and fast voltage-sensitive dye imaging. Dynamic characterization of the spontaneous IBs showed that they originated in dentate gyrus/CA3 border and propagated toward CA1. To determine how β-AR modulates spatiotemporal characteristics of the emergent IBs, we used the β-AR agonist isoproterenol (ISO). ISO significantly reduced the spatiotemporal extent and propagation velocity of the IBs and significantly altered network activity in the 1- to 20-Hz range. Dual whole cell recordings of the IBs in CA3/CA1 pyramidal cells and optical analysis of those regions showed that ISO application reduced interpyramidal and interregional synchrony during the IBs. In addition, ISO significantly reduced duration not only of the shorter duration IBs but also the prolonged ILEs in 4-AP. To test whether the decrease in ILE duration was model dependent, we used a different hyperexcitability model, zero magnesium (0 Mg^{2+}). Prolonged ILEs were readily formed in 0 Mg^{2+}, and addition of ISO significantly reduced their durations. Taken together, these novel results provide evidence that β-AR activation dynamically reshapes the spatiotemporal activity patterns in hyperexcitable circuits by altering network rhythmogenesis, propagation velocity, and intercellular/regional synchronization.

neuromodulation; neural circuits; epilepsy; adrenergic

A NUMBER OF NEUROLOGICAL DISORDERS are accompanied by changes in the levels of neuromodulators or their respective binding receptors (Caiati et al. 2010; Hablitz 2004; Khorkova and Golowasch 2007; Lenz et al. 1997; Rutecki 1995; Svensson et al. 2001; Vaughan and Christie 2005; Weinshenker and Szot 2002). In some instances increases in the endogenous levels of neuromodulators can control neuronal network hyperexcitability and the associated pathophysiologies (Bandyopadhyay and Hablitz 2007; Kong et al. 2010). For example, thousands of patients with intractable forms of epilepsy have implants for vagus nerve stimulation (VNS) (El Tahry et al. 2010; Elliott et al. 2011; Lund et al. 2011; McLachlan 1997; Vale et al. 2010). Although not a sole effect, VNS in patients and in animals elevates levels of norepinephrine (NE) in the brain. This additional NE is thought to be anticonvulsive (Giorgi et al. 2004; Krahl et al. 1998; Roosevelt et al. 2006; Szot et al. 1999, 2001; Weinshenker and Szot 2002).

In the brain, noradrenergic fibers densely innervate polymorphic hippocampal, neocortical, and cerebellar tissues (Cox et al. 2008; Giorgi et al. 2004; Grant and Redmond 1981; Milner et al. 2000; Weinshenker and Szot 2002). Actions of NE are mediated by α-adrenergic (α-AR) and β-adrenergic receptors (β-AR) and their respective subtypes (Mueller and Dunwiddie 1983; Mueller et al. 1981, 1982; Weinshenker and Szot 2002). α-AR mostly has been shown to be anticonvulsive, but a number of studies have described β-AR as both pro- and anticonvulsive (Clinckers et al. 2010; Ferraro et al. 1994; Ko et al. 1984; Mueller et al. 1981; Weinshenker and Szot 2002; Weinshenker et al. 2001). Nonetheless, it is not known how β-AR modulates global synchronized circuit dynamics during spontaneous activity or in commonly used pathological hyperexcitability models.

Fast functional imaging techniques with high spatiotemporal resolution reveal that neuromodulators can remap evoked neural network activation patterns (Bandyopadhyay and Hablitz 2007; Mann et al. 2005; Pena and Ramirez 2004; Svensson et al. 2001). A combination of single-cell electrophysiology and fast imaging techniques (Carlson and Coulter 2008; Coulter et al. 2011) can now allow us to probe the role of neuromodulators in altering neural activity patterns and intercellular synchronization (Dzirasa et al. 2010; Fernandez de Sevilla et al. 2006; Puig et al. 2010). Thus it is important to use this combination of these techniques to determine emergent neural network dynamics and their modulation on cell-to-cell and network levels.

To examine the β-adrenergic control of excitability and synchrony, we used robust models of epileptogenic hyperexcitability and integrated electrophysiology, fast voltage-sensitive dye imaging (VSDI), and image analysis tools. Dynamic characterization of the synchronized spontaneous interictal bursts (IBs) and ictal-like events (ILEs) in single cells or pairs of cells, pace-making zones, and the interconnected hippocampal circuits showed that the β-AR agonist isoproterenol (ISO) has anti-ictal qualities. We present new evidence that ISO reorganizes spatiotemporal topology of spontaneous hypersynchronous neuronal activity. We

Address for reprint requests and other correspondence: J. Žiburkus, Dept. of Biology and Biochemistry, Univ. of Houston, 4800 Calhoun Rd. SR2 Rm. 349, Houston, TX 77204-5001 (e-mail: jziburkus@uh.edu).

show that this topological rearrangement of IBs is accompanied by intercellular and interregional desynchronization, decreases in signal propagation velocity, modulation of specific frequency components across the microcircuits, and reduction in the ILE durations.

MATERIALS AND METHODS

Hippocampal slice preparation. All of the experiments were performed following experimental guidelines approved by University of Houston Institutional Animal Care and Use Committee. Transverse hippocampal brain slices were prepared from male Sprague-Dawley rats (postnatal *days 21–27*). The rats were anaesthetized with ether and decapitated, and the brains were rapidly excised and placed in oxygenated (95% O_2-5% CO_2), ice-cold dissection buffer solution containing (in mM) 212.7 sucrose, 2.5 KCl, 1.25 NaH_2PO_4, 3 $MgSO_4$, 10 $MgCl_2$, 0.5 $CaCl_2$, 26 $NaHCO_3$, and 10 dextrose. Hippocampal slices (350 μm) were prepared using a Vibratome (Technical Products International) and preincubated for 0.5 h in normal artificial cerebrospinal fluid (ACSF; pH 7.3, 30°C) containing (in mM) 130 NaCl, 1.2 $MgSO_4$, 3.5 KCl, 1.2 $CaCl_2$, 10 glucose, 2.5 NaH_2PO_4, and 24 $NaHCO_3$ aerated with 95%O_2-5%CO_2.

Voltage-sensitive dye staining of hippocampal slices. After preincubation, 60 μl of voltage-sensitive dye (VSD) stock solution were spread over the slice surfaces using small-tip pipettes with a final dye concentration of 0.03 mg/ml. Slices were incubated in ACSF with the dye for an hour before recording began (Carlson and Coulter 2008; Tominaga et al. 2000). We used two types of VSD: amino-naphthyl-ethenylpyridinium dye 4 and dye 8 (di-4ANEPPS and di-8ANEPPS, respectively). Di-8ANEPPS was used in a subset of experiments to confirm the presence of inhibitory currents and hyperpolarizations (Mennerick et al. 2010). In the presence of both di-4 and di-8ANEPPS dyes, viable bursting responses and seizures were observed (Mapelli et al. 2010; Tominaga and Tominaga 2010), and results from the two dyes were grouped together for the final analysis. The fractional change in fluorescence signal ($\Delta F/F_{max}$) in our data was calculated by comparing the change in the intensity of fluorescence (ΔF) in each pixel relative to the maximum intensity of background fluorescence (F_{max}). Identical gain and threshold parameters were used when comparing optical data in all experimental conditions. The same $\Delta F/F_{max}$ values are used for analysis and representation of our VSD data, including static image frames and Supplemental Movies S1–S3. (Supplemental data for this article is available online at the *Journal of Neurophysiology* website.)

Electrophysiology. After the incubation, slices were placed in a submersion chamber (Warner Instruments) in an upright wide-field epifluorescence microscope (BX51WI; Olympus) equipped with a complementary metal-oxide semiconductor (CMOS) camera for VSD imaging (Ultima-L; BrainVision, SciMedia) and a infrared-differential interference contrast (IR-DIC) camera (Dage MTI) for visualized whole cell recordings. During concurrent electrophysiological recording and imaging, the slices were continuously perfused (2 ml/min, at 30°C) with oxygenated ACSF containing (in mM) 130 NaCl, 0.6 $MgSO_4$, 3.5 KCl, 0.6 $CaCl_2$, 10 glucose, 2.5 NaH_2PO_4, and 24 $NaHCO_3$. Electrical recording electrodes were pulled from borosilicate thin-walled glass tubes (IB150-4; World Precision Instruments, Sarasota, FL) using a micropipette puller (P97; Sutter Instruments). Extracellular or whole cell recordings were performed concurrently with the VSD imaging. Extracellular field or whole cell membrane potentials were recorded concurrently from CA3 and CA1 areas. Extracellular electrodes (resistance 1–2 MΩ, filled with 0.9% saline) were placed near the apical tufts of pyramidal cell dendrites (stratum radiatum). For the whole cell current-clamp recordings, borosilicate glass micropipettes (4–7 MΩ) contained (in mM) 116 K-gluconate, 6 KCl, 0.5 EGTA, 20 HEPES, 10 phosphocreatine, 0.3 NaGTP, 2 NaCl, 4 MgATP, and 0.3% neurobiotin (pH 7.25, 295 mosmol/ml). Pyramidal cell membrane properties were assessed from the voltage responses to a series of 500- to 1,000-ms hyper- and depolarizing current steps incremented by 25 to 50 pA. Dual whole cell recordings for cross-correlation measures were performed in pairs of CA3 and CA1 pyramidal cells. All electrical recordings were performed using MCC 700 amplifiers (Axon Instruments). Electrical data were low-pass filtered at 4 kHz, digitized at 10 kHz (Digidata; pCLAMP; Molecular Devices).

Spontaneous IBs and ILEs were induced with 50 μM 4-aminopyridine (4-AP) added to the ACSF, constantly maintained at 34°C (Avoli 1990). 4-AP increases hyperexcitability of inhibitory and excitatory cells via the block of the transient A- and D-type K^+-mediated currents (Storm 1987; Thompson 1982; Traub et al. 1995). Both IBs and ILEs comprise increased inhibitory and excitatory conductances and their interplay (Aradi and Maccaferri 2004; Rutecki et al. 1987; Žiburkus et al. 2006). To confirm that the effect of the β-AR modulator was model independent, in addition we used a 0-Mg^{2+} model. The resistance of ictal events to pharmacological manipulations in 4-AP and 0 Mg^{2+} has been proposed to model pharmacoresistant forms of epilepsy (Albus et al. 2008; D'Antuono et al. 2010; Fueta and Avoli 1992; Wahab et al. 2010). To modulate spontaneous epileptiform activity, we activated β-AR with agonist (ISO; 10 μM) (Emorine et al. 1989; Jurgens et al. 2005; Lands et al. 1967). ISO was added 20 min after application of 4-AP. In most cases, only IBs form and persist within 20 min of 4-AP application (Žiburkus et al. 2006). Typically, longer time duration or a higher concentration of added 4-AP is needed to induce prolonged ILEs (Avoli 1990; Žiburkus et al. 2006). However, in a number of slices 4-AP formed ILEs earlier, and in these cases we were able to measure electrically the effects of ISO on ILE durations. In the prolonged presence of 4-AP, network hyperexcitability typically increases for the period of 1.5–2 h, continuously evoking combination of recurrent IBs and prolonged ILEs.

In the prolonged presence of 4-AP or 0 Mg^{2+}, network hyperexcitability typically increases steadily and evokes a combination of IBs and ILEs beyond the time duration of our recordings. Thus the modulatory effects of ISO were not due to activity or tissue rundown. All drugs were bath-applied following dilution into ACSF from stock solutions and were perfused during experiments. Chemicals were purchased from Sigma (St. Louis, MO) and Tocris (Ellisville, MO).

Imaging spontaneous activity with VSDs. Before recording spontaneous activity, we performed studies using electrical stimulation of the Schaeffer collaterals and calibrated electrical responses with optical images. We also performed control studies on the photo bleaching effects of the dye and tissue viability (data not shown). Dye bleaching was less than 5% during a total light exposure time of 2 min. The total time of all of the acquired frames for our experiments was typically 10 acquisitions of 4–8 s. To characterize spontaneous spatiotemporal propagation patterns, we performed optical recordings over the entire hippocampal slices (Supplemental Movie S1). Stained slices were illuminated with an electronic shutter-controlled 150-W halogen light source (Moritex) and passed through a filter cube [excitation wavelength (λ) = 530 ± 10 nm, dichroic λ = 565 nm, and absorption λ > 590 nm; U-MWIG2, Olympus] (Tominaga et al. 2000). Full-frame (100 × 100 pixels) image acquisition was performed at 0.5–1 kHz with the CMOS camera (Ultima-L; BrainVision, SciMedia). Each camera pixel with a ×4 objective (Olympus; NA 0.28) corresponds to 25 μm^2. To capture the initial bursts, we performed continuous electrical recordings and simultaneously listened to the voltage through a sound amplifier. As soon as the early signs of epileptogenic activity were detected, we initiated the timed manual sampling of spontaneous burst data (4–8 s/acquisition) within the first minute of bursting with a minimum of 30 s (and a maximum of 1 min) for interevent recovery. Typically, the initial bursts emerged ~3–5 min after bath application of 4-AP. To assure absolute electro-optical instrument synchronization, optical and electrical data acquisition was triggered with a Digital stimulator (PG4000A; Cygnus Technology) and, additionally, electrical signals were acquired with

the optical analog-to-digital converter. Supplemental Movies S1–S3 were created by exporting the acquired images into a video format using BrainVision (SciMedia) software and truncating them for shorter playback time using Adobe Premiere Professional software.

Morphological confirmation of recorded neurons. Whole cell patch pipette solution contained 0.3% neurobiotin (Vector Labs, Burlington, ON, Canada), and at the end of the recording, the slices were fixed for 48 h at 4°C in 4% paraformaldehyde. During staining, the slices were recovered from paraformaldehyde by thorough washing in phosphate-buffered saline and were treated with an avidin-biotin-peroxidase complex (ABC kit; Vector), rinsed, and reacted with diaminobenzidine tetrahydrochloride and H_2O_2. Subsequently, the sections were mounted on glass slides, and photographs and reconstructions were performed using a confocal microscope.

Data analysis. Electrophysiology analysis was done using either Clampfit (pCLAMP 10.2; Molecular Devices) or Matlab (The MathWorks) software. Extracellular spontaneous bursts were identified using the threshold search function in Clampfit, and the bursts were analyzed for the measurements of the interevent intervals and durations of the spontaneous events. All of the optical analysis was performed on files that were high-pass filtered (0–500 Hz).

Continuous wavelet transform analysis. To determine the power of dominant frequency during spontaneous bursting phase in 4-AP and 4-AP + ISO (see Fig. 1), we performed time-frequency analysis using the continuous wavelet transform (CWT) (Huberfeld et al. 2011). Normalized Morlet wavelet scales ($\omega_0 = 6$) were chosen to reflect the unit frequencies across 0–50 Hz using a basis function of the form

$$\text{Scale} = \frac{\omega_0 + \sqrt{2 + \omega_0^2}}{4\pi f}. \quad (1)$$

For CWT analysis, regions of interests (ROIs) were constructed in anatomically defined CA1 and CA3 regions containing similar numbers of pixels (500 ± 5–10 pixels). Average differential fluorescent signals of individual pixels from respective ROIs were treated as single-channel data and further used for the computation of the CWT. The resulting wavelet-based spectrogram plot represents signal power at each frequency as a function of time, with the use of a color map (corresponding to scale) where warmer colors represent larger magnitudes (i.e., larger scales).

Propagating burst characterization. Optical data were analyzed using either BrainVision (SciMedia) or custom-written algorithms in Matlab. To determine whether ISO application reduced burst propagation from CA3 into CA1, the normalized optical data were averaged over pixels to obtain a temporal signal for each recording, in each ROI (CA3 and CA1), and under each condition (4-AP and 4-AP + ISO; see Fig. 5). Bursts were detected in the CA3 signals by first smoothing with a Gaussian kernel and then searching for times at which the derivative was positive and exceeded the mean of the absolute value of the derivative by more than 2 SD. We analyzed 20 frames before and 120 frames after the burst. For each burst, we then calculated the relative change in peak activity as Δ = peak CA1/peak CA3. Optical burst velocities (see Fig. 5) were determined with a three-point Bézier curve along the trajectory of the signal propagation. Optical velocity measurements were later verified with measurements of latency in electrical signal between extracellular electrode pairs placed in CA3 and CA1 (see Fig. 3). Propagation decay and velocity values were statistically compared using Student's *t*-test.

Fourier transform analysis. Fourier transforms (FTs) were computed with average differential fluorescent signals ($\Delta F/F$) of individual pixels from respective ROIs constructed over CA3 and CA1 (see Fig. 4). To calculate the FT of a signal, $x(t)$, a backwards version of the signal was first concatenated onto itself,

$$X(t) = x(t) \text{ for } 0 \le t \le T \text{ and } X(t) = x(T - t/2) \text{ for } T < t \le 2T. \quad (2)$$

This practice eliminates the contamination of the FT by long timescale trends in the data, such as experimental drift. The power spectrum was obtained by computing the square of the absolute value of the FT. Average FT analysis was performed on the optical signal in the 1- to 50-Hz range. This range was further divided into 10-Hz sections: 1–10, 10–20, 20–30, 30–40, and 40–50 Hz.

Cell-to-cell and interregional cross-correlations. To monitor synchrony between individual CA3-CA1 cell pairs, we performed dual whole cell patch-clamp recordings (see Fig. 9). CA3 and CA1 cell spike train cross-correlation values were calculated as follows: spike times from paired electrical recordings of CA1 and CA3 were detected using a membrane voltage threshold of −15 mV. For each paired recording, raw cross-correlation at lag t was computed as mean firing rate of CA1 neurons t units of time after a spike in CA3. Each raw cross-correlation was then normalized as in *Eq. 3*, where $r1$ and $r3$ are the average firing rates of the CA1 and CA3 neurons, respectively. This yields a dimensionless measure of dependence between the spike trains.

$$C_{\text{norm}}(t) = \frac{C_{\text{raw}}(t) - r1r3}{\sqrt{r1r3}}. \quad (3)$$

To measure regional synchrony between CA3 and CA1, we used the "xcov" function in Matlab with the option "coeff" to calculate the cross-correlation between the fluorescence measured at pairs of pixels chosen from the two ROIs. The cross-correlation at lag τ calculated in this manner is equivalent to the offset Pearson correlation coefficient,

$$C_{xy}(\tau) = \frac{\text{cov}[x(t), y(t+\tau)]}{\sqrt{\text{var}[x(t)]\text{var}[y(t)]}}, \quad (4)$$

where covariances and variances are obtained by averaging values over time.

Global spatial entropy measurements. To determine the change in synchrony over the entire tissue, we used an image segmentation approach and computed the global spatial entropy (see Fig. 11). Entropy measures the information context of the entire VSD signal, which includes fast sub- and suprathreshold neuronal membrane potential fluctuations. Uniform distribution of activity is expressed as a high entropy level. Conversely, low entropy is calculated when activity becomes organized in small regions. To calculate the spatial entropy of an imaged area at a given time t, the squared fluorescence of each pixel was normalized as

$$y_j(t) = \frac{x_j^2(t)}{\sum_{l=1}^{N} x_i^2(t)}, \quad (5)$$

where $x_j(t)$ is the fluorescence recorded at the jth pixel at time t. The spatial entropy is then defined as the entropy of the distribution of squared fluorescence,

$$H(t) = -\sum_{j=1}^{N} y_j(t)\log_2[y_j(t)]. \quad (6)$$

Statistical analysis was performed with Prism software (version 5; GraphPad Software).

RESULTS

Fast optical imaging of spontaneous bursts in the hippocampal circuits. To study emergent hippocampal circuit activity and synchrony, we used the 4-AP model of hyperexcitability (50 μM). In vitro, 4-AP reliably evokes short-duration synchronized bursts, often referred to as interictal bursts (IBs), and longer duration ictal-like events (ILEs), typically seen at higher concentrations of 4-AP (100–200 μM) (Žiburkus et al. 2006). Overall, the emergence of hyperexcitability was found to initiate within 4–5 min following bath application of 4-AP.

Shorter duration bursts formed reliably and persisted in all of the stained slices, indicating good tissue viability and a robust physiology of the stained hippocampal circuits. We were able to monitor individual spontaneous burst activity using electrophysiology and fast VSDI simultaneously (Fig. 1, *A–C*; Supplemental Movie S1). Simultaneous extracellular and whole cell recordings in the CA3 and CA1 areas and VSDI of the entire hippocampal slice were performed (Carlson and Coulter 2008; Sinha and Saggau 2001).

First, we dynamically characterized the spatiotemporal patterns of IBs. We determined the sites of spontaneous burst origins. Optical data analysis based on threshold detection (MATERIALS AND METHODS) indicated that a great majority of the bursts (~95%) in the hyperexcitable network originate in the dentate gyrus (DG)/CA3 border and propagate down the trisynaptic pathway into CA1 and subicullum (Sinha and Saggau 2001). Representative data from five rats ($n = 50$ bursts, 5 slices) are shown in Fig. 1*C*, with the cytoarchitectural outline of the hippocampus and burst origin sites marked and overlaid (Adobe Photoshop CS3). The initiation and propagation of the signal were additionally confirmed by analyzing the electrical delay in the extracellular electrical traces simultaneously recorded from CA3 and CA1 (see Fig. 5*H*). Similar to temporal lobe epilepsy models, where the DG "gate" is compromised, here formation and propagation of the residual activity in the hippocampal slice are also widespread (Carlson and Coulter 2008; Sinha and Saggau 2001).

β-Adrenergic modulation of spatiotemporal patterns and cellular rhythmogenesis. To test the effects of β-AR activation on spontaneous spatiotemporal pattern formation, network hyperexcitability, and synchrony, we used ISO. CWT analysis of the electrical and optical signals in the ROIs showed that epileptogenic burst activity recorded in CA3 and CA1 contained power over a wide spectrum of the low-frequency and higher frequency components (0–50 Hz; Figs. 2 and 3). We specifically focused on the 1- to 50-Hz frequency range, which includes theta and lower end gamma frequencies (Buzsaki et al. 2004). Application of ISO significantly reduced power in both the electrical and optical signals. When equal size ROIs from CA3 and CA1 were analyzed using Fourier transforms and averaged over pixels, significant reductions were observed in the CA1 region (Fig. 4). The strongest effect was in the 1- to 20-Hz range ($P < 0.0313$), suggesting that the spatial remapping by ISO acts by altering activity in the delta, theta, and beta ranges, and not within the low gamma rhythm range (30–50 Hz) (Katsuki et al. 1997).

Further optical analysis additionally showed that ISO reduced the spatial extent of spontaneous IB propagation (Figs. 3 and 5; Supplemental Movies 2 and 3, see MATERIALS AND METHODS). The spatial spread (Fig. 5, *A–D*) and propagation velocity (Fig. 5, *E–G*) of epileptiform bursts in 4-AP and 4-AP + ISO were quantified. Addition of ISO significantly decreased the spatial spread and propagation velocity of IBs from CA3 to CA1. Effects of burst spatial confinement and temporal variability were not time dependent, and robust epileptiform activity can be sustained in 4-AP for hours (Avoli 1990; Žiburkus et al. 2006). In neocortical tissue, traveling neural activity wave velocities have been shown to range from 0.01 to 0.5 m/s (Connors and Amitai 1997; Pinto et al. 2005; Sanchez-Vives and McCormick 2000). In our tests, ISO reduced the propagation velocity of IBs from CA3 to CA1 from 0.3085 ± 0.013 to 0.1622 ± 0.006 m/s (means ± SE; $P \leq 0.03$; $n = 60$ IBs, $N = 6$ rats; Fig. 5*G*). This reduction in

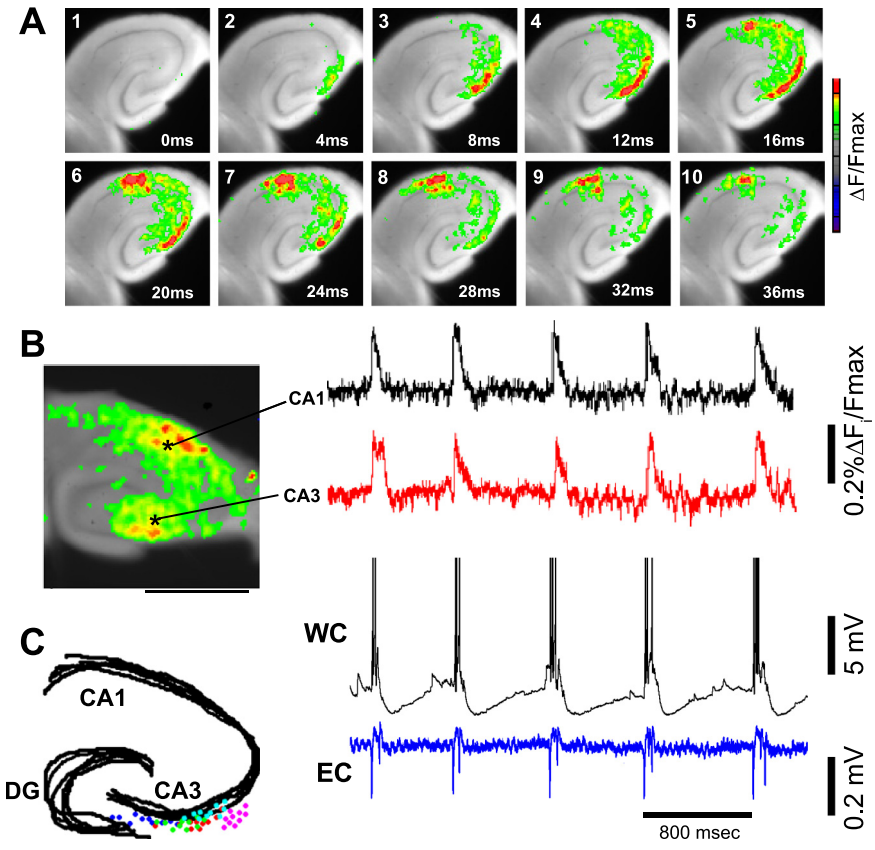

Fig. 1. Spatiotemporal patterns of synchronized electrical bursts in the hippocampus. *A*: sequential frames (1–10) of a single unfiltered burst recorded optically. Luminescence of di-4-ANEPPS is linearly correlated with the neuronal membrane potential fluctuations. Amplitude of the voltage-sensitive dye (VSD) responses is indicated by the color scale (blue, hyperpolarization; red, depolarization). $\Delta F/F_{max}$, fractional change in fluorescence signal. *B*: spatiotemporally averaged optical signals of a representative interictal burst (IB). Optical traces were taken from individual representative pixels in areas CA3 and CA1. *Top right*: corresponding $\Delta F/F_{max}$ traces from representative pixels near the zone of burst initiation in the CA3 area. *Bottom right*: simultaneous whole cell (WC) and extracellular (EC) recordings obtained during the optical imaging of the bursts. Note that optical burst duration was almost identical to those seen during whole cell membrane potential shifts. Nonetheless, WC, EC, and VSD recordings are likely sampling signals from different-sized regions. *C*: sketches of the hippocampus outlines. Black lines indicate the cellular dentate gyrus (DG) and cornus ammoni (CA) areas. Superimposed are the dots indicating the sites of synchronized burst origins in those samples (50 bursts, 5 rats). Burst origins were derived using threshold analysis, which detects the earliest and strongest pixels activated preceding the burst propagation and spread (BrainVision; see MATERIALS AND METHODS).

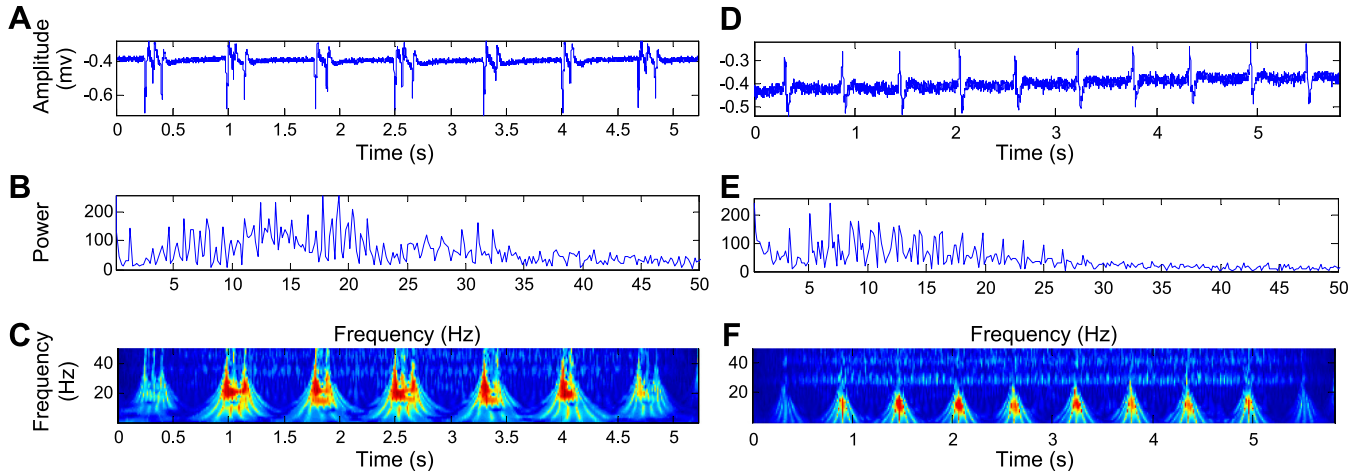

Fig. 2. Isoproterenol (ISO) modulates dominant frequencies of the electrically recorded IBs. *A*: repetitive IBs recorded extracellularly in CA3 pyramidal cell layer in the presence of 50 μM 4-aminopyridine (4-AP). *B*: average Fourier transform (FT) shows an average power over the presented time series of the IBs shown in *A*. Power is in arbitrary units. *C*: continuous wavelet transform (CWT) spectrogram of the IBs shown in *A*. CWT plots represent power spectrum over time. IBs contain signal power within a broad (low and high) frequency range. *D*: IBs from *A* following application of ISO. ISO reduced the duration of electrically recoded 4-AP-induced IBs in the hippocampal slice. *E* and *F*: FT and CWT analysis of the IBs from *D*. ISO drastically diminished the power of electrical signal in high and low frequencies.

propagation velocity was additionally verified by measuring the delay of electrical traces recorded in CA3 and CA1 (4-AP: 9.183 ± 0.35 ms; 4-AP + ISO: 29.02 ± 0.46 ms; $P < 0.0001$; Fig. 5*H*). Given that the distance between extracellular recording electrodes is ~2.5–3 mm (Fig. 5*F*), the electrical latency values are in agreement with the propagation velocity values obtained from the optical recordings. These results suggest that ISO slows the communication between the two interconnected hippocampal circuits, CA3 and CA1, and also reshapes the dynamics of voltage activation footprint.

Additionally, when extracellular electrical traces were measured, ISO significantly reduced the duration of IBs seen in 4-AP alone (from 325.3 ± 7.67 to 243.0 ± 6.84 ms; $P = < 0.0001$, $n = 128$ bursts, $N = 5$ rats; Fig. 6, *A* and *B*). To further

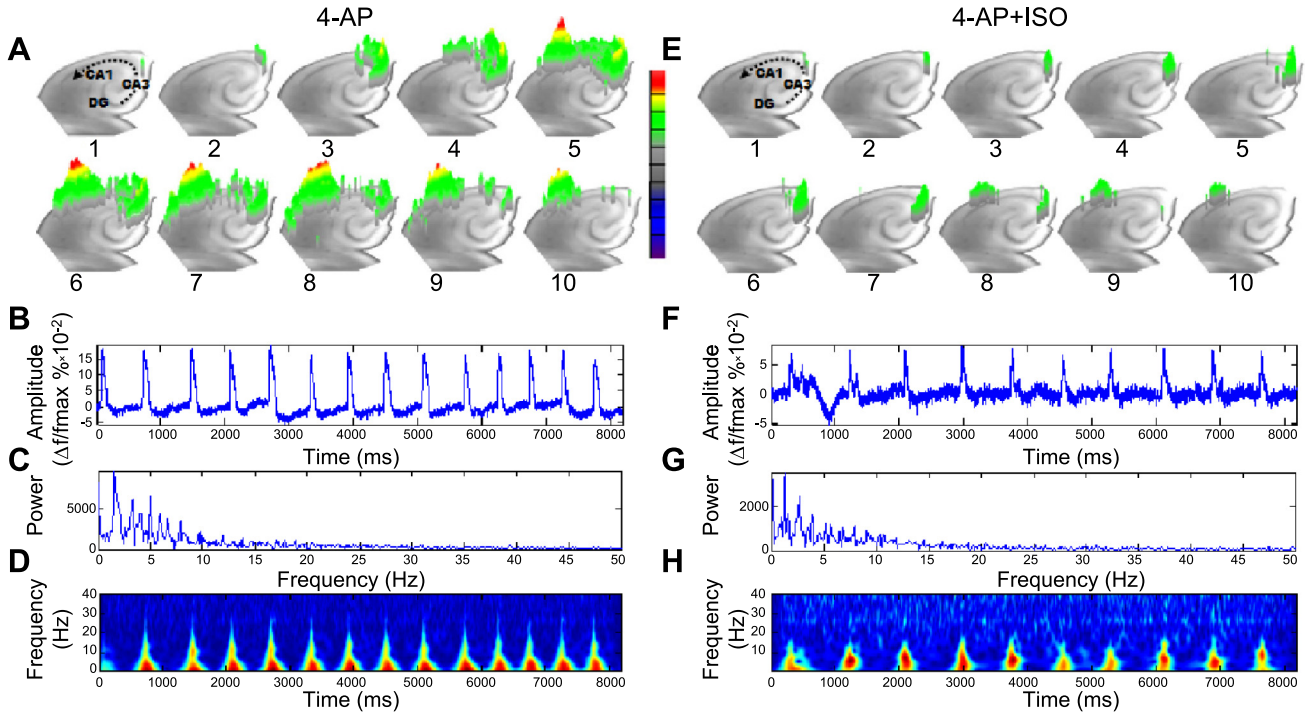

Fig. 3. ISO sculpts the spatiotemporal characteristics of the optically recorded IBs. *A*: sequential photo frames (every 5 ms) showing VSD signals of a single IB in 3-D. 4-AP evoked propagating bursts that originated in the CA3/DG border and propagated to CA1. Color bar: red indicates the strongest depolarization. Dotted line indicates the direction of the IB propagation in the trisynaptic DG-CA3-CA1 hippocampal pathways. Images shown are at 5-ms intervals to demonstrate the complete IB propagation. Acquisition rate, 500 Hz. *B*: average optical traces from the region of interest (ROI) in the CA3 region (500-pixel average $\Delta F/F_{max}$). *C*: FT diagram showing the dominant power of the optical signals. On average, optical signals recorded during the bursts were longer in duration than the electrical traces (Fig. 1). *D*: CWT analysis plots of the repetitive IBs shown in *B*. *E*: when ISO was added to the bath solution containing 4-AP, the spatial extent of neuronal activation map during the IBs was reduced. *F*: average optical ROI signal in the 4-AP + ISO condition. *G*: average FT analysis as in *C*, but for the 4-AP + ISO condition. *H*: CWT analysis of the modulated bursts shows attenuation in signal power at low frequencies.

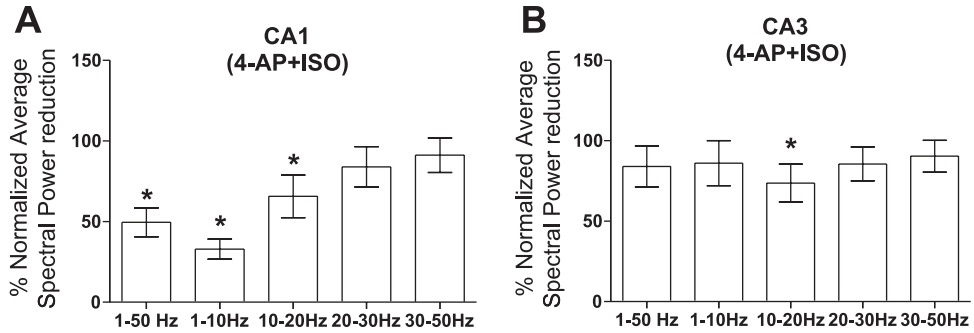

Fig. 4. ISO modulates 0- to 20-Hz frequencies of the synchronous activity. *A* and *B*: average FFT power plots of optical data from CA1 (*left*) and CA3 (*right*) ROIs ($n = 5$ slices) showing changes in the average power in the range of 1–50 Hz band during application of 4-AP and 4-AP + ISO. Discrete plots represent the total power spectrum broken up into 10-Hz-range sections that incorporate the following oscillatory rhythms: delta and theta (~1–4 and 4–10 Hz), alpha and beta (10–15 and 15–30 Hz), and gamma frequency (30–50 Hz). After addition of ISO, the most significant difference in voltage power, on average, was observed at ranges of 1–10 and 10–20 Hz in the CA1 region. Values are means ± SE. $^*P < 0.0313$, Wilcoxon matched pairs signed rank test.

determine the effect of β-AR activation on network rhythmogenesis, we measured interburst interval (IBI) durations in extracellular and whole cell recordings. ISO introduces greater variability in the occurrence of IBs recorded extracellularly (Fig. 6, *C* and *D*) and in whole cells (see Fig. 9). This type of neural arrhythmia is a possible mechanism by which neuromodulators could rearrange spatiotemporal maps of highly synchronous neural activity or of those reflecting synaptic plasticity in neural circuits.

β-Adrenergic modulation of ILEs. Although our electro-optical protocols were designed to monitor IB activity, within 10 min of application of 4-AP, a number of slices ($n = 12$ slices) started generating ILEs (see MATERIALS AND METHODS, *Electrophysiology* and Fig. 6; see also Avoli 1990; Netoff et al.

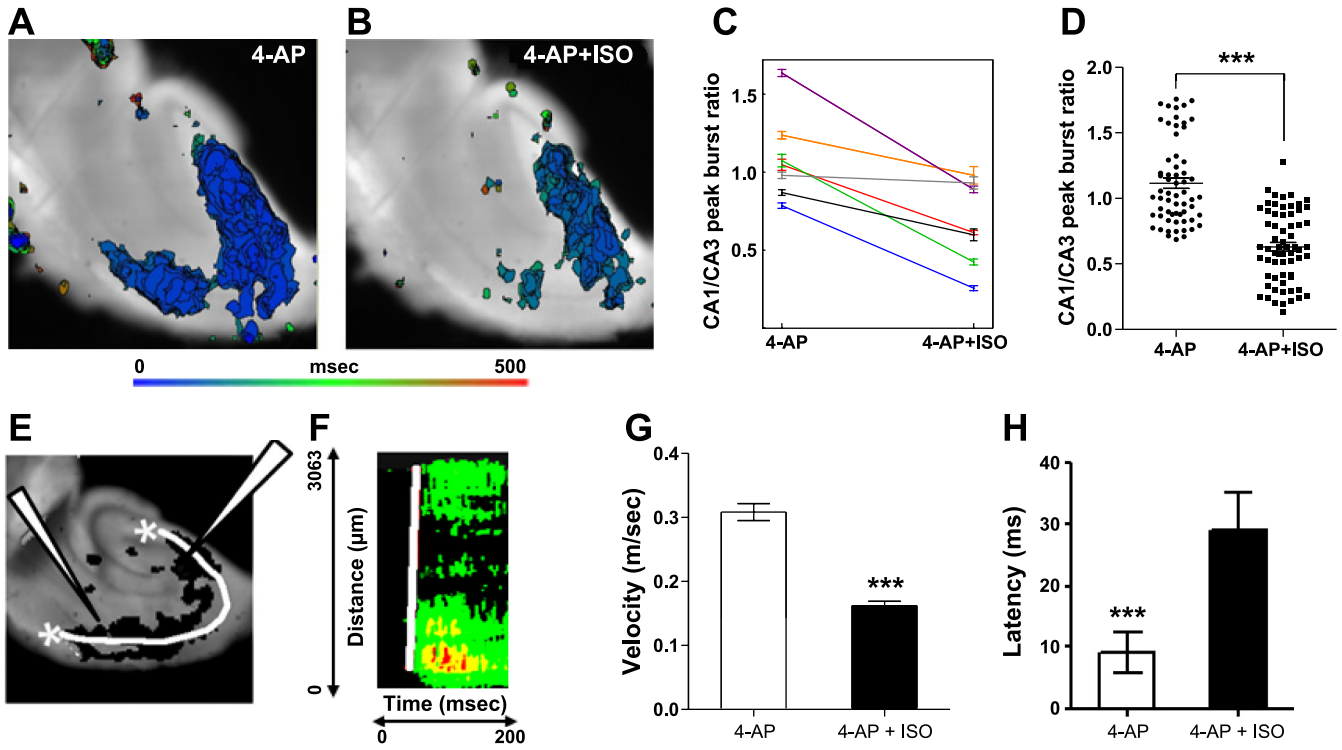

Fig. 5. ISO modulates propagation of the synchronized bursts. *A* and *B*: average neural map activation during a typical IB in 4-AP (*A*) and 4-AP + ISO (*B*). The spatial extent of signal activation was drastically reduced when ISO was added to 4-AP. Aside from the areal activation, the spatial maps also contain temporal information: blue color indicates the fastest activity spread (4-AP), whereas green and red indicate slow activation (4-AP + ISO). *C*: CA1-to-CA3 peak amplitude ratio of the burst shows a significant decrease after addition of ISO. Each color plot represents individual slice examples in 4-AP and 4-AP + ISO ($n = 7$ slices, 8–10 bursts/slice). *D*: averages and SE for all 7 slices in *C* (64 bursts total). $^{***}P < 0.0001$, indicating that, on average, addition of ISO caused a significant decrease in the amplitude of the propagating bursts from CA3 to CA1. *E*: illustration of velocity calculations along the path of IB propagation from CA3 to CA1 areas. Asterisks indicate the start and the end of line that is superimposed on the path of the propagating signal (black). Two extracellular electrodes were used to concurrently record field potentials in CA3 and CA1. *F*: flattened 2-D plot of the propagating IB. The signal (green and red colors) gets aligned in time over the distance of the line from CA3 to CA1. Rightward tilted white line shows the temporal delay between the earliest detectable signals in CA3 (*bottom*) and CA1 (*top*). *G*: velocity of IB in 4-AP (0.3 m/s) was reduced (0.16 m/s) during coapplication of ISO. $^{***}P < 0.03$, Wilcoxon signed rank test. Data represent measurements of the speed of synchronized burst propagation from the individual slices in 4-AP and 4-AP with ISO. *H*: measurements of electrical delay (latency) between CA3 and CA1 extracellular electrodes ($n = 7$ slices). $^{***}P < 0.0001$, Wilcoxon signed rank test. Optically measured velocity and electrical delay both indicate that ISO slows down signal propagation from CA3 into CA1.

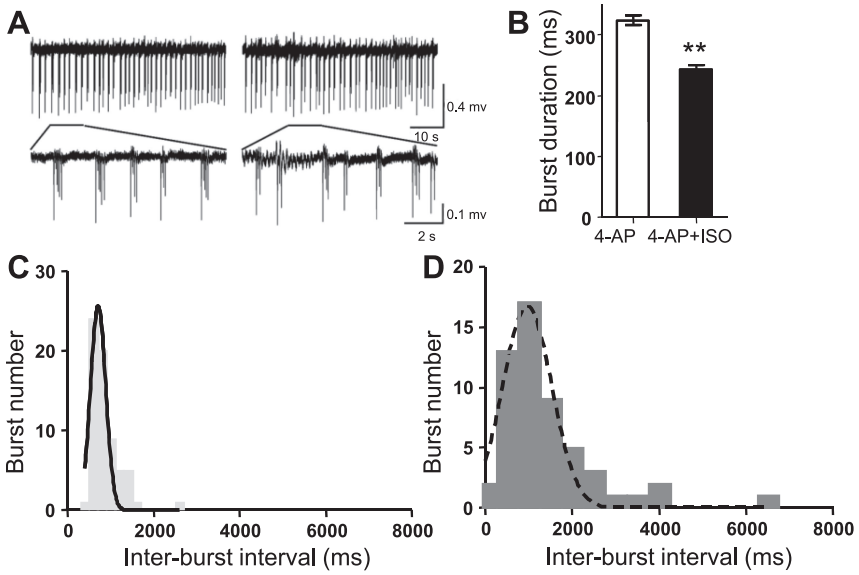

Fig. 6. ISO reduces burst durations and increases interburst interval (IBI) variability. *A*: synchronized burst traces recorded extracellularly. *B*: in the presence of ISO, burst duration decreased from an average of 325.3 ± 7.67 to 243.2 ± 6.84 ms. Values are means ± SE. $^{**}P < 0.0001$. *C*: in the presence of 4-AP, the IBI was very regular, as reflected by the distribution histogram (fitted with Gaussian curve). Regression value = 0.8337. *D*: ISO increased the IBI variability, resulting in the broader distribution histogram and the fitted curve. Regression value = 0.9340.

2002; Schiff et al. 2008; Žiburkus et al. 2006). In those instances, ISO was applied and electrical ILE activity was recorded without imaging (to avoid photobleaching during the prolonged ILEs). Figure 7 shows that application of ISO significantly reduced duration of the ILE events in both the CA3 and CA1 regions in 4-AP (from 44.79 ± 1.79 to 18.90 ± 1.11 ms; $P < 0.002$). In some instances ($n = 4$), ISO caused ILEs to cease.

Blockade of 4-AP-evoked ILEs encouraged us to look at another robust hyperexcitability and seizure model, 0 Mg^{2+} (Fig. 8) (Huberfeld et al. 2011). In contrast to the 4-AP model, which acts by blockade of potassium currents, prolonged ILEs in 0 Mg^{2+} result from increased opening of NMDA receptor and decreased membrane charge screening (Avoli et al. 1987; Derchansky et al. 2004; Huberfeld et al. 2011; Mody et al. 1987; Traub et al. 1994). Robust bursting and ILEs formed readily in the presence of 0 Mg^{2+} (Fig. 8). Despite the fact that the two models have distinct cellular mechanisms, addition of ISO to 0-Mg^{2+} ACSF significantly reduced the duration of ILEs (from 88.29 ± 2.96 to 51.61 ± 2.90 ms; $P < 0.0005$, $n = 5$ slices, $N = 5$ rats). Furthermore, as is evident in Fig. 8, ISO increased the number of bursts preceding ILEs. IBs often preempt ictal events and are thought to drive this system into a subsequent prolonged synchronization (Huberfeld et al. 2011; Schiff et al. 2008). In vivo seizures and in vitro ILEs are often associated with focal increases in synchrony levels (Dauwels et al. 2009; Huberfeld et al. 2011; Jiruska et al. 2010; Jouny et al. 2010; Perreault and Avoli 1991; Prida and Sanchez-Andres 1999; Žiburkus et al. 2006). Seizure duration often indicates phenotype severity, and a substantial body of theoretical and experimental work indicates that increased and prolonged excitatory network synchronization causes longer duration seizures (Žiburkus et al. 2006). In our experiments, increased interburst variability (Fig. 6) and duration of preictal phase suggest that in the ISO-modulated conditions, a greater number of bursts are necessary to drive this system into ILEs (Figs. 7 and 8). This in turn suggests that ISO modulates spatiotemporal hyperexcitability patterns by desynchronizing

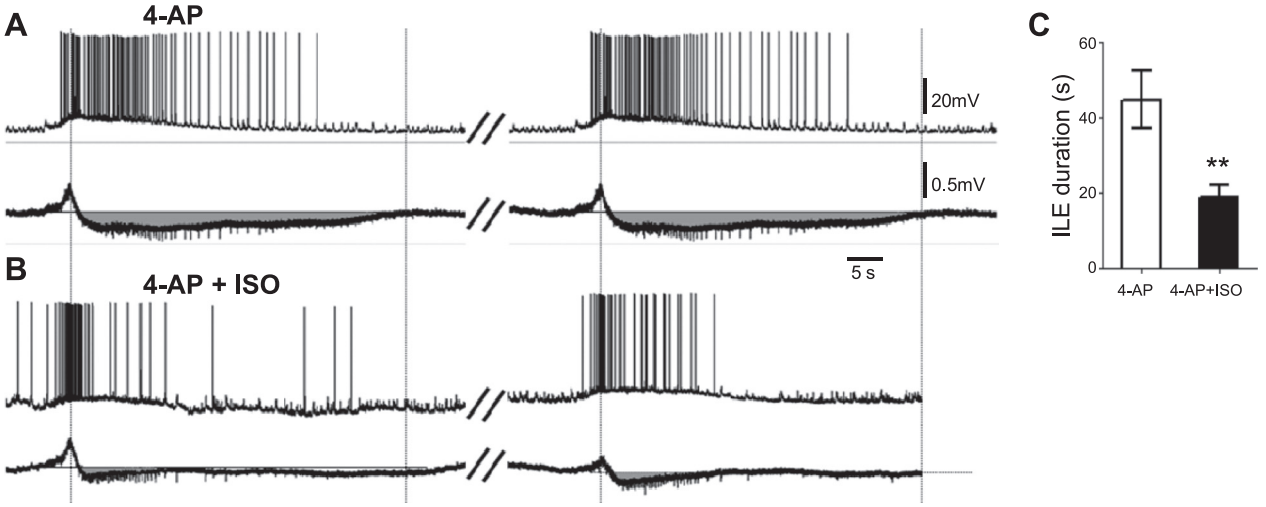

Fig. 7. ISO reduces duration of the ictal-like events (ILEs) in 4-AP. *A*: concurrent WC recordings from pyramidal cells and EC recordings of consecutive seizure-like events (SLEs) in the CA3. Unfiltered DC recording mode traces are shown. ILEs are represented by the prolonged depolarization with the typical high-frequency "ringing" activity. *B*: ictal durations were significantly reduced following application of ISO. *C*: bar graph showing the average reduction in ILE duration following addition of ISO. Values are means ± SE ($n = 19$ slices). $^{**}P < 0.002$.

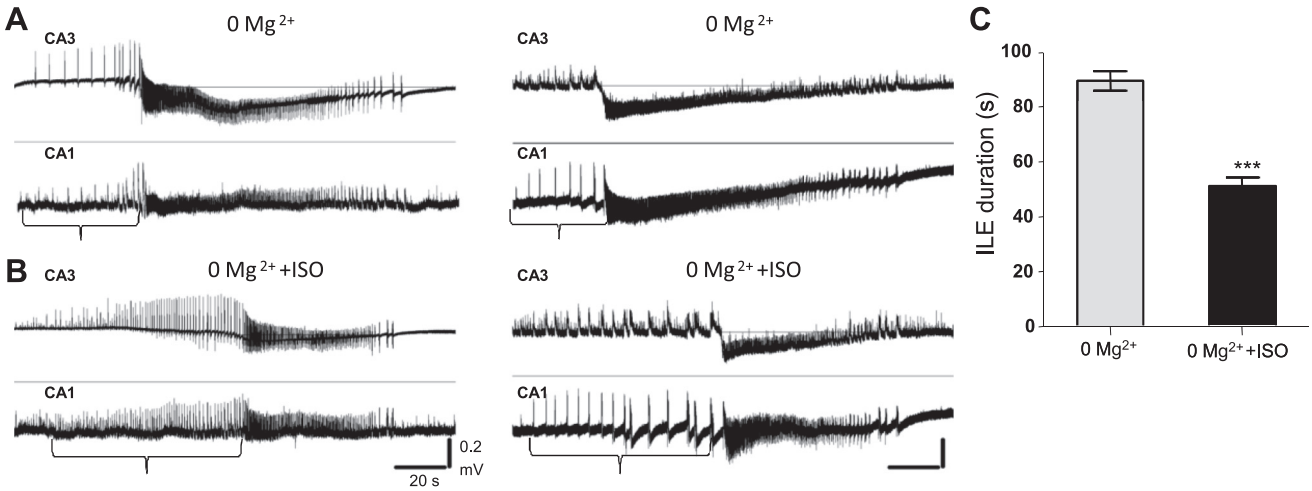

Fig. 8. ISO reduces duration of the ILEs in 0 Mg^{2+}. *A*: unfiltered electrical traces of SLEs from 2 (*left* and *right*) representative dual EC recordings performed in the CA1 and CA3 regions in 0-Mg^{2+} artificial cerebrospinal fluid. *B*: application of ISO (0 Mg^{2+} + ISO) reduced ILE duration and increased the number of bursts during the pre-ictal phase (inverted brackets). *C*: bar graph showing the average ILE duration in 0 Mg^{2+} and 0 Mg^{2+} + ISO. ISO significantly decreased ILE duration (from 89.68 ± 3.67 to 51.15 ± 3.247 s). Values are means ± SE (n = 5 slices). ***$P < 0.0001$.

focal circuits and extended hippocampal networks, not unlike previous observations in vivo (Dzirasa et al. 2010).

β-Adrenergic activation modulates cellular and regional synchrony. To determine how cellular and network synchrony changed in epileptogenic and modulated conditions, we recorded from pairs of CA3 and CA1 pyramidal cells and analyzed corresponding optical files containing the same synchronized bursts. Figure 9 illustrates that ISO modulates the epileptogenic state by breaking up the even rhythmic burst pattern established by 4-AP and reducing the cross-correlation values between individual CA3 and CA1 cells within a narrow sliding temporal window (10 ms). The drop in cell-to-cell cross-correlation (Fig. 9*C*) is also consistent with the increases in burst time variability mediated by ISO (Fig. 6). To characterize synchronization between the interconnected CA3 and CA1 circuits that had clearly propagating bursts, we used optical recordings. Normalized cross-correlation measures over the ROIs in the CA3 and CA1 regions showed a dramatic decrease in the presence of ISO (Fig. 10). The regional analysis suggests that the loss of interregional synchronization could potentially be reflected on an even larger scale, namely, the entire hippocampal slice in the field of view.

Global spatial entropy analysis demonstrated that there is a significant reduction in the entropy levels during the individual spontaneous IBs in 4-AP (Fig. 11). Such reduction in entropy levels were previously only reported during seizures with the use of multi-electrode arrays (Jiruska et al. 2010; Raiesdana et al. 2009). In the present study, when ISO was added, network entropy levels were increased, suggesting an overall decrease in hippocampal CA3-CA1 synchronization (Fig. 11, *B* and *C*). The levels of relative decrease in entropy values were comparable in 4-AP and 4-AP + ISO (Fig. 11*D*). Taken together, local and global synchronization measurements suggest that β-AR activation may abrogate pathological hyperexcitability via intercellular, interregional, and global system desynchronization.

DISCUSSION

We present new evidence that β-AR modulates spontaneous hyperexcitable neural activity patterns in hippocampal circuits.

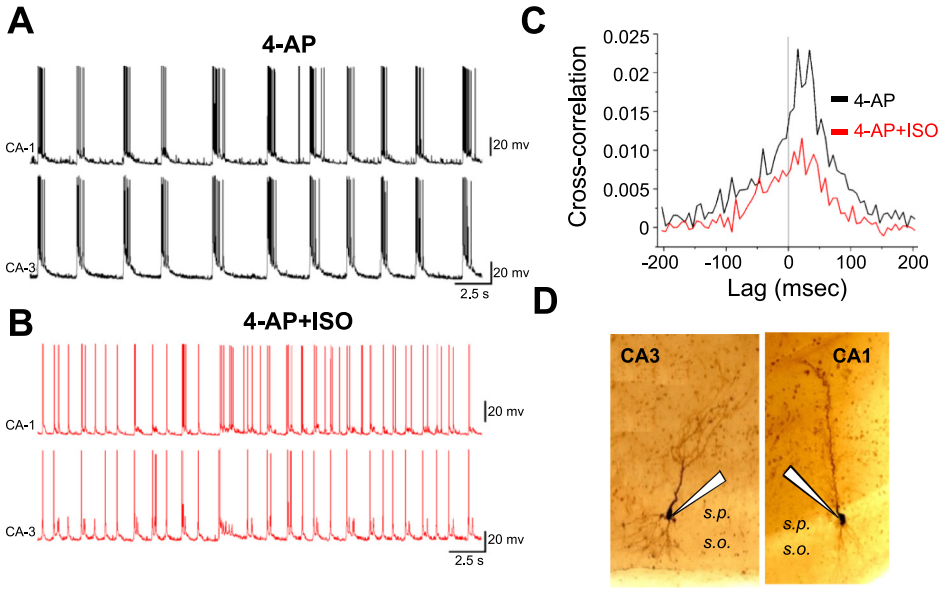

Fig. 9. β-Adrenergic modulation of spike synchrony between CA3 and CA1 cells. *A* and *B*: electrical traces from dual WC recordings from a pair of CA3 and CA1 pyramidal cells. ISO was added before SLEs formed; note that the periodically occurring prolonged bursts in 4-AP were broken up into a shorter duration and less regular bursting pattern. *C*: average cross-correlation measurements indicating that ISO reduces intercellular spike synchrony between CA3 and CA1 pyramidal cells. $P \leq 0.0001$ (n = 4,000 spikes, N = 6 slices). *D*: examples of reconstructed photomicrographs showing the recorded pyramidal cells from CA3 and CA1 (s.p., stratum pyramidale; s.o., stratum oriens).

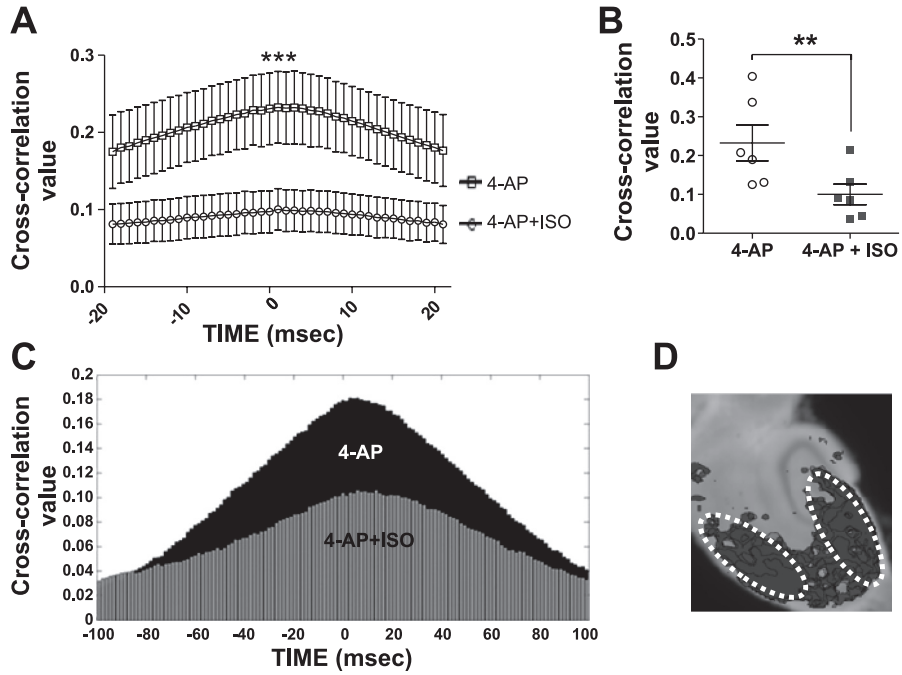

Fig. 10. β-Adrenergic modulation of interregional synchrony. *A*: average cross-correlation values between the CA3 and CA1 regions during bursts in 4-AP and 4-AP + ISO. The *top* 3 peak values were statistically compared to confirm a highly significant reduction (0.2076 ± 0.0028 to 0.09064 ± 0.0009 ms). Values are means ± SE ($n = 6$ slices). ***$P < 0.0001$. *B*: overall average cross-correlation values calculated from *A* (0.2325 ± 0.0464 to 0.1003 ± 0.0268 ms). Values are means ± SE. **$P < 0.0063$. *C*: bar graph representation of the cross-correlation values over a longer window than in *A* for a representative CA3-CA1 cell pair. *D*: photomicrograph showing the locations of the ROIs (1,000 pixels are outlined by the dotted ellipses) used to calculate interregional synchronization.

β-AR agonist confined the spatial extent of spontaneous synchronized bursts. We show that this confinement is accompanied by increased variability and desynchronization of single cells and interconnected ROIs, modulation of low-frequency bands in a region-specific manner, and changes in propagation velocity of the synchronized signal. One mechanism by which VNS is thought to reduce seizure frequency in clinically refractory patients is through upregulation of NE. Our results support the possibility that NE activation of β-AR in the seizure-prone hippocampus may be anticonvulsant. Circuit level analysis shows that β-AR's anticonvulsant effects are in part mediated by a reduction in synchrony, extent of spatial circuit activation, and modulation of neural activity propagation velocity. In parallel with the modulatory attributes of β-AR in the hyperexcitable states, other neuromodulators may also sculpt spatiotemporal patterns of normal ongoing neuronal activity in an analogous way.

Fast functional imaging of synchronized neuronal activity. In otherwise quiet brains, the hyperexcitable states of activation are both a product and a target of endogenous neuromodulators. Because synchronized activity is a network phenomenon, fast functional imaging offers unique abilities to observe and study spatiotemporal neural activation patterns and their modulation (Chemla and Chavane 2010; Coulter et al. 2011; Grinvald and Hildesheim 2004; Wu et al. 2008; Zecevic et al. 2003). Propagating waves of activity can be observed in vivo and in vitro in a variety of preparations and under a variety of experimental conditions (Chemla and Chavane 2010; Connors and Amitai 1997; Daaka et al. 1997; Lubenov and Siapas 2009; Morozov et al. 2003; Sanchez-Vives and McCormick 2000). Epileptiform waves serve as an excellent model of synchronized propagating activity because they can arise both spontaneously (Weissinger et al. 2005) and through evoked electrical stimulation in the presence of inhibitory blockers (Pinto et al. 2005). To date, however, only a handful of studies have methodically characterized spatiotemporal dynamics during spontaneously arising epileptogenic activity (Gonzalez-Sulser et al. 2011). Most of the studies evoked waves via electric stimulation, inevitably imposing a certain spatial activation pattern on the underlying circuit. However, when emergent network activation was imaged, previously unseen aspects of spatiotemporal dynamics, such as origin sites of synchronized bursts, their vectors of propagation, and even local, layer-specific inhibitory activity, were detected (Sinha and Saggau 2001; Weissinger et al. 2005). In agreement with previous electrical studies (Avoli et al. 1988; Gonzalez-Sulser et al. 2011; Traub et al. 1995, 1996), we observed that synchronized bursts originated in the DG/CA3 area and propagated down the trisynaptic hippocampal pathway. In some instances, after the IB emergence in a small zone in the CA3, the signal spread within the broader area in the CA3 and toward the DG. Pyramidal cells in the CA3 are highly interconnected, and our results suggest that small pacemaker-like zones may exist within this area. Using fast VSDI, we dynamically characterized features of the initial, spontaneously propagating bursts, such as velocity, spatial activation maps, and regional synchronization. These synchronized bursts in the hippocampus travel with velocity comparable to neocortical waves (Connors and Amitai 1997; Pinto et al. 2005; Sanchez-Vives and McCormick 2000). We further showed that β-AR activation can modulate velocity and other dynamical characteristics of these waves.

Activity-dependent modulation of distinct neural network frequencies. Excitability of neuronal networks is modulated by diffuse subcortical projections that release neuromodulators such as acetylcholine, dopamine, and NE (Dzirasa et al. 2010; Hablitz 2004; Kobayashi et al. 2000; Reddy 2010). Neuromodulators shape the overall behavioral state and may promote or curtail specific oscillation frequencies in vivo and in vitro (Buzsaki 2006; Hablitz 2004; Huang et al. 1996). Several studies point to the fact that normal NE activity in vivo and in vitro is critical for modifying cross-structural activation (Dzirasa et al. 2010) or serves as an anticonvulsant in VNS patients. In vivo, NE was shown to largely modulate theta frequencies (Dzirasa et al. 2010; Oestreich et al. 2007), but its modulatory

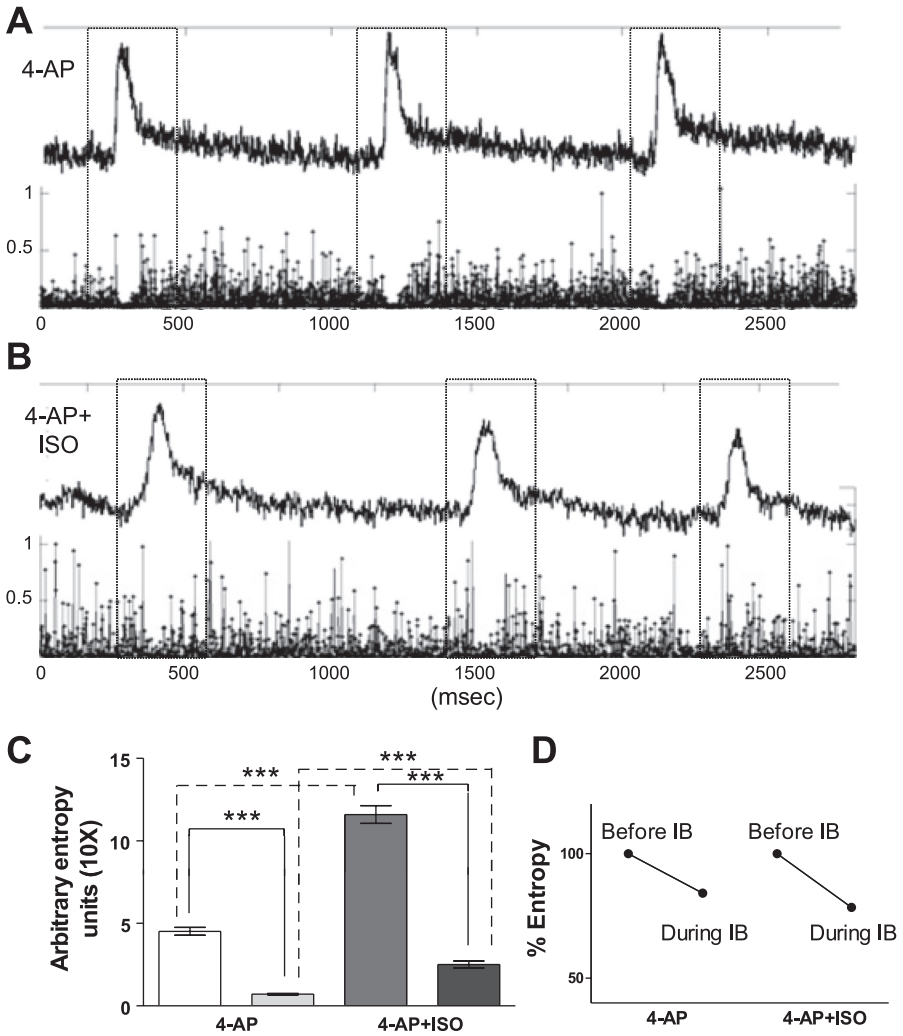

Fig. 11. β-Adrenergic modulation of global network synchrony. *A*: representative pixel with the optical traces (*top*) of repetitive bursts recorded in the CA1 region. Scatter plots (*bottom*) are examples of the continuous global entropy values as a function of the bursts. *B*: traces and entropy measures from *A* after application of ISO. *C*: average peak values (*left* bar for each condition) preceding the drop in entropy (*right* bar for each condition) associated with the IBs. Greater entropy levels were present after addition of ISO. Values are means ± SE ($n = 6$ slices, 48 bursts): 4-AP peak vs. drop, 4.521 ± 0.235 to 0.7142 ± 0.042; 4-AP + ISO peak vs. drop, 11.60 ± 0.536 to 2.502 ± 0.212; 4-AP vs. 4-AP + ISO peak, 4.521 ± 0.235 to 11.60 ± 0.536; 4-AP vs. 4-AP + ISO drop, 0.7142 ± 0.042 to 2.502 ± 0.212. ***$P < 0.0001$. *D*: drop in entropy expressed as a percentage demonstrates kinetically equivalent drops in epileptogenic and β-adrenergic modulated conditions.

mechanisms during VNS are unknown. Remarkably, our results showed that β-AR agonist ISO also curtails and redistributes the power of low frequencies, including theta range during the synchronized bursts. This suggests that the earlier reported NE effects on theta rhythms (Dzirasa et al. 2010; Oestreich et al. 2007) may be predominantly modulated via β-AR, thereby confining or specifying cross-modal topology. In addition, β-AR activation reduces the propagation velocity of synchronized bursts between the CA3 and CA1 regions, potentially desynchronizing the distally connected circuits and leaving a stronger activity imprint locally.

Most recently, it was reported that NE and ISO modulate sharp wave-ripple (SPW-R) activity in the hippocampus (Ul Haq et al. 2011). Electrical stimulation-induced repetitive SPW-Rs contained most of their spectral power in high frequencies (100–400 Hz). NE decreased and ISO increased SPW-R occurrence. High-frequency oscillations observed in human and animals are thought to play key roles in fast epileptiform network synchronization (Huberfeld et al. 2011). The underlying changes in spectral bands observed here could also be indicative of the heightened or dampened activity in distinct cell subpopulations (Cox et al. 2008). It is important to add that in the 4-AP model of developing mouse tissue, ionotropic glutamate or GABA receptor blockade resulted in significant alterations of spontaneous burst propagation patterns measured electrically (Gonzalez-Sulser et al. 2011). These and our findings imply that adrenergic modulation of specific frequency bands is dependent on the dynamical nature of the ongoing activity (evoked vs. spontaneous and SPW-Rs vs. bursts or ILEs), anatomy, and receptor subtype activation. Further investigations are necessary to determine the precise mechanisms by which other neuromodulators affect various frequency components of synchronized activity and how this modulation depends on activity and anatomy.

β-AR modulation of cellular and network synchrony. β-AR activation with ISO is required to evoke certain forms of spike timing-dependent plasticity (STDP) in the hippocampus and neocortex. Distinct classes of neuromodulators acting through their intracellular cascades can also differentially regulate STDP, or the "learning curves" (Seol et al. 2007). Because neuromodulators can control the activation of plastic brain states, their impact on network synchrony and activity is fundamental, but it remains largely unexplored. Our findings suggest that pathway-specific strengthening in associative synaptic plasticity could be reflected by the spatial rearrangement in activity patterns or even confinement reported here. Nonetheless, the ability to "zoom in and out" of the activated and modulated cells and circuits exposes new levels of complexity of synchronous network interactions. For example, previous electrophysiology studies characterized a novel excitatory-

inhibitory cell (E-I) interplay during synchronized bursts and seizure-like events in the CA1 region (Aradi and Maccaferri 2004; Fujiwara-Tsukamoto et al. 2004; Žiburkus et al. 2006). We showed that E-E, but not E-I, spike cross-correlations increased during the seizures in CA1 (Žiburkus et al. 2006). Buno et al. showed that hyperexcitable CA3 pyramidal cells decorrelate their firing in the presence of ISO. These studies targeted cells in one area of the hippocampus (CA1 or CA3) and lack the details of spatiotemporal activation maps. Our current study shows that spike desynchronization between individual CA3 and CA1 cells is accompanied by a variety of network mechanisms, including the loss of interregional and global synchrony.

In multi-electrode recordings in hippocampal slices, global synchrony (using a global entropy measure) increased at the onset of in vitro ILEs (Jiruska et al. 2010). What is notable in our results is that global entropy is significantly reduced during individual IBs, which are much shorter in duration and smaller in their spatial extent than ictal events. Additionally, ISO applied in the presence of either 4-AP or 0 Mg^{2+} drastically increased the number of bursts that preceded ILEs. ISO further modulated the levels of entropy, reducing synchrony during bursts. If preictal bursts are indicative of levels of system synchrony, then an increased number of preictal bursts and decreased synchronization during the bursts suggest that ISO desynchronizes the system (hippocampal slice) (Hasko et al. 2008; Huberfeld et al. 2011). In the modulated condition, it therefore takes many more attempts (preictal bursts) for the same system to get primed and synchronize to form longer duration ILEs. The changes that we observed in the entropy levels correlated well with the decrease in the interregional and intercellular cross-correlations.

Once the ILEs are initiated in 4-AP and 0 Mg^{2+}, the prolonged seizure dynamics can be sustained and exacerbated over a period of up to 2 h (Barbarosie and Avoli 1997; Calcagnotto et al. 2000; Žiburkus et al. 2006). Here the effects of ISO were tested following just two to three initial seizures in 4-AP or 0 Mg^{2+}. On average, these seizures showed relatively uniform ictal duration times (see MATERIALS AND METHODS and Žiburkus et al. 2006), and when ISO was applied, the ILE (like the IB) durations decreased significantly. It remains to be determined whether the washout of β-adrenergic agonist can again return network dynamics into the premodulated state. However, it is likely that the initial effects of ISO observed here are mediated through longer lasting changes in G protein-coupled molecular and ionic conductances.

Molecular and ionic basis of adrenergic modulation. We have shown that ISO rearranges spatiotemporal hyperexcitable network patterns and abrogates epileptiform activity. This suggests that neuromodulators modulate or impart distinct spatiotemporal patterns in a receptor-specific manner. ISO initiates β-receptor G protein-coupled cascades leading to changes in ionic conductances, such as potassium (Gouder et al. 2003). In particular, it is an effective blocker of the medium and late afterhyperpolarizations (AHPs) (Fernandez de Sevilla et al. 2006; Madison and Nicoll 1986; Pedarzani and Storm 1996). The prolonged AHPs have been implicated in ictogenesis and may be necessary to synchronize the hippocampal cells (Fernandez de Sevilla et al. 2006). It may at first seem paradoxical that the broadening of action potentials by 4-AP increases synchrony and that blockade of AHP by ISO reduces synchrony. However, prolonged AHPs may provide the synchronized inhibitory quench and proper sodium channel de-inactivation that would further promote repetitive seizure activity. On the other hand, the effects of ISO on AHP may be more pronounced on the inhibitory cells (Cox et al. 2008; Milner et al. 2000), alleviating spike adaptation in the GABAergic networks and resulting in reduced global synchronization. It is becoming more evident that inhibitory activity and inhibitory conductances are often necessary for global network synchronization (Hu et al. 2011; Schiff et al. 2008; Uhlhaas et al. 2009; Van Vreeswijk et al. 1994) and seizure induction (Žiburkus et al. 2006). Finally, ISO has also been shown to block gap junctions in the neurogliaform cells (Zsiros and Maccaferri 2008). Together, effects of ISO on increased firing variability and blockade of fast electrical transmission could contribute to the anticonvulsant actions we observed.

At a membrane, ISO could act through β_1- and β_2-receptor subtypes (Crissman et al. 2001; Tang et al. 1998). On the other hand, NE released by VNS or by subcortical nuclei activation would also activate the α-AR subtypes (Zhong and Minneman 1999). It is likely that in our studies the observed effects were mediated by β_1-and β_2-receptors. Additional studies with β_1-, β_2-, and α-AR subtype-specific agonists and antagonist are needed to delineate their distinct anti- and proconvulsant mechanisms.

On the molecular side, several studies have shown that actions of β-AR signaling can be mediated through either cyclic AMP protein kinase A (PKA)-dependent (Daaka et al. 1997) or -independent (Oestreich et al. 2007) molecular signaling. These independent pathways activate mitogen-activated protein kinase and lead to increased phosphorylation of extracellular signal-regulated kinase (pERK), a molecule crucial for certain forms of learning and memory (Morozov et al. 2003). 4-AP also upregulates ERK phosphorylation through unknown cellular mechanisms, suggesting a cause-effect relationship between levels of pERK and ictogenesis. We suggest that regulation of molecular ERK via β-AR cascades also affects network synchrony and neural activity propagation. This fundamental intracellular signaling cascade is at the crossroads of ictogenesis (Merlo et al. 2004), synchrony, and synaptic plasticity (Seol et al. 2007). Finally, 4-AP and 0 Mg^{2+} serve as models of intractable epilepsy, and the molecular evidence suggests that pathways leading to ERK phosphorylation should be further explored as potential therapeutic targets for epilepsy.

ACKNOWLEDGMENTS

We thank Aditya Barua, Trupti Wadadekar, Ahmad Aulakh, Lena Nguyen, Ngan Nguyen, and Linda Abad for technical assistance; Drs. Richard Bond, Steven J. Schiff, and Stuart Dryer for discussions of the manuscript; and Dr. Jason Eriksen for use of the confocal microscope.

GRANTS

This research was supported by the Epilepsy Foundation of America (J. Žiburkus and A. Hazra), National Science Foundation Grants DMS-0604429 and DMS-0817649, and the Texas Advanced Research Program/Advanced Technology Program (K. Josić and R. Rosenbaum).

DISCLOSURES

No conflicts of interest, financial or otherwise, are declared by the authors.

AUTHOR CONTRIBUTIONS

Author contributions: A.H. and J.Ž. performed experiments; A.H., R.R., B.B., S.C., K.J., and J.Ž. analyzed data; A.H. and J.Ž. prepared figures; A.H. and J.Ž. drafted manuscript; A.H., R.R., K.J., and J.Ž. edited and revised manuscript; A.H., R.R., B.B., K.J., and J.Ž. interpreted results of experiments; J.Ž. and A.H. conception and design of research; J.Ž. approved final version of manuscript.

REFERENCES

Albus K, Wahab A, Heinemann U. Standard antiepileptic drugs fail to block epileptiform activity in rat organotypic hippocampal slice cultures. *Br J Pharmacol* 154: 709–724, 2008.

Aradi I, Maccaferri G. Cell type-specific synaptic dynamics of synchronized bursting in the juvenile CA3 rat hippocampus. *J Neurosci* 24: 9681–9692, 2004.

Avoli M. Epileptiform discharges and a synchronous GABAergic potential induced by 4-aminopyridine in the rat immature hippocampus. *Neurosci Lett* 117: 93–98, 1990.

Avoli M, Louvel J, Pumain R, Olivier A. Seizure-like discharges induced by lowering $[Mg^{2+}]_o$ in the human epileptogenic neocortex maintained in vitro. *Brain Res* 417: 199–203, 1987.

Avoli M, Perreault P, Olivier A, Villemure JG. 4-Aminopyridine induces a long-lasting depolarizing GABA-ergic potential in human neocortical and hippocampal neurons maintained in vitro. *Neurosci Lett* 94: 327–332, 1988.

Bandyopadhyay S, Hablitz JJ. Dopaminergic modulation of local network activity in rat prefrontal cortex. *J Neurophysiol* 97: 4120–4128, 2007.

Barbarosie M, Avoli M. CA3-driven hippocampal-entorhinal loop controls rather than sustains in vitro limbic seizures. *J Neurosci* 17: 9308–9314, 1997.

Buzsaki G. *Rhythms of the Brain*. New York: Oxford University Press, 2006.

Caiati MD, Sivakumaran S, Cherubini E. In the developing rat hippocampus, endogenous activation of presynaptic kainate receptors reduces GABA release from mossy fiber terminals. *J Neurosci* 30: 1750–1759, 2010.

Calcagnotto ME, Barbarosie M, Avoli M. Hippocampus-entorhinal cortex loop and seizure generation in the young rodent limbic system. *J Neurophysiol* 83: 3183–3187, 2000.

Carlson GC, Coulter DA. In vitro functional imaging in brain slices using fast voltage-sensitive dye imaging combined with whole-cell patch recording. *Nat Protoc* 3: 249–255, 2008.

Chemla S, Chavane F. Voltage-sensitive dye imaging: technique review and models. *J Physiol Paris* 104: 40–50, 2010.

Clinckers R, Zgavc T, Vermoesen K, Meurs A, Michotte Y, Smolders I. Pharmacological and neurochemical characterization of the involvement of hippocampal adrenoreceptor subtypes in the modulation of acute limbic seizures. *J Neurochem* 115: 1595–1607, 2010.

Connors BW, Amitai Y. Making waves in the neocortex. *Neuron* 18: 347–349, 1997.

Coulter DA, Yue C, Ang CW, Weissinger F, Goldberg E, Hsu FC, Carlson GC, Takano H. Hippocampal microcircuit dynamics probed using optical imaging approaches. *J Physiol* 589: 1893–1903, 2011.

Cox DJ, Racca C, LeBeau FE. Beta-adrenergic receptors are differentially expressed in distinct interneuron subtypes in the rat hippocampus. *J Comp Neurol* 509: 551–565, 2008.

Crissman AM, Makhay MM, O'Donnell JM. Discriminative stimulus effects of centrally administered isoproterenol in rats: mediation by beta-1 adrenergic receptors. *Psychopharmacology (Berl)* 154: 70–75, 2001.

D'Antuono M, Kohling R, Ricalzone S, Gotman J, Biagini G, Avoli M. Antiepileptic drugs abolish ictal but not interictal epileptiform discharges in vitro. *Epilepsia* 51: 423–431, 2010.

Daaka Y, Luttrell LM, Lefkowitz RJ. Switching of the coupling of the beta2-adrenergic receptor to different G proteins by protein kinase A. *Nature* 390: 88–91, 1997.

Dauwels J, Eskandar E, Cash S. Localization of seizure onset area from intracranial non-seizure EEG by exploiting locally enhanced synchrony. *Conf Proc IEEE Eng Med Biol Soc* 2009: 2180–2183, 2009.

Derchansky M, Shahar E, Wennberg RA, Samoilova M, Jahromi SS, Abdelmalik PA, Zhang L, Carlen PL. Model of frequent, recurrent, and spontaneous seizures in the intact mouse hippocampus. *Hippocampus* 14: 935–947, 2004.

Dzirasa K, Phillips HW, Sotnikova TD, Salahpour A, Kumar S, Gainetdinov RR, Caron MG, Nicolelis MA. Noradrenergic control of cortico-striato-thalamic and mesolimbic cross-structural synchrony. *J Neurosci* 30: 6387–6397, 2010.

El Tahry R, Raedt R, Mollet L, De Herdt V, Wyckuys T, Van Dycke A, Meurs A, Dewaele F, Van Roost D, Doguet P, Delbeke J, Wadman W, Vonck K, Boon P. A novel implantable vagus nerve stimulation system (ADNS-300) for combined stimulation and recording of the vagus nerve: pilot trial at Ghent University Hospital. *Epilepsy Res* 92: 231–239, 2010.

Elliott RE, Morsi A, Kalhorn SP, Marcus J, Sellin J, Kang M, Silverberg A, Rivera E, Geller E, Carlson C, Devinsky O, Doyle WK. Vagus nerve stimulation in 436 consecutive patients with treatment-resistant epilepsy: Long-term outcomes and predictors of response. *Epilepsy Behav* 20: 57–63, 2011.

Emorine LJ, Marullo S, Briend-Sutren MM, Patey G, Tate K, Delavier-Klutchko C, Strosberg AD. Molecular characterization of the human beta 3-adrenergic receptor. *Science* 245: 1118–1121, 1989.

Fernandez de Sevilla D, Garduno J, Galvan E, Buno W. Calcium-activated afterhyperpolarizations regulate synchronization and timing of epileptiform bursts in hippocampal CA3 pyramidal neurons. *J Neurophysiol* 96: 3028–3041, 2006.

Ferraro G, Sardo P, Sabatino M, La Grutta V. Locus coeruleus noradrenaline system and focal penicillin hippocampal epilepsy: neurophysiological study. *Epilepsy Res* 19: 215–220, 1994.

Fueta Y, Avoli M. Effects of antiepileptic drugs on 4-aminopyridine-induced epileptiform activity in young and adult rat hippocampus. *Epilepsy Res* 12: 207–215, 1992.

Fujiwara-Tsukamoto Y, Isomura Y, Kaneda K, Takada M. Synaptic interactions between pyramidal cells and interneurone subtypes during seizure-like activity in the rat hippocampus. *J Physiol* 557: 961–979, 2004.

Giorgi FS, Pizzanelli C, Biagioni F, Murri L, Fornai F. The role of norepinephrine in epilepsy: from the bench to the bedside. *Neurosci Biobehav Rev* 28: 507–524, 2004.

Gonzalez-Sulser A, Wang J, Motamedi GK, Avoli M, Vicini S, Dzakpasu R. The 4-aminopyridine in vitro epilepsy model analyzed with a perforated multi-electrode array. *Neuropharmacology* 60: 1142–1153, 2011.

Gouder N, Fritschy JM, Boison D. Seizure suppression by adenosine A1 receptor activation in a mouse model of pharmacoresistant epilepsy. *Epilepsia* 44: 877–885, 2003.

Grant SJ, Redmond DE Jr. The neuroanatomy and pharmacology of the nucleus locus coeruleus. *Prog Clin Biol Res* 71: 5–27, 1981.

Grinvald A, Hildesheim R. VSDI: a new era in functional imaging of cortical dynamics. *Nat Rev Neurosci* 5: 874–885, 2004.

Hablitz JJ. Regulation of circuits and excitability: implications for epileptogenesis. *Epilepsy Curr* 4: 151–153, 2004.

Hasko G, Linden J, Cronstein B, Pacher P. Adenosine receptors: therapeutic aspects for inflammatory and immune diseases. *Nat Rev Drug Discov* 7: 759–770, 2008.

Hu H, Ma Y, Agmon A. Submillisecond firing synchrony between different subtypes of cortical interneurons connected chemically but not electrically. *J Neurosci* 31: 3351–3361, 2011.

Huang CC, Hsu KS, Gean PW. Isoproterenol potentiates synaptic transmission primarily by enhancing presynaptic calcium influx via P- and/or Q-type calcium channels in the rat amygdala. *J Neurosci* 16: 1026–1033, 1996.

Huberfeld G, Menendez de la Prida L, Pallud J, Cohen I, Le Van Quyen M, Adam C, Clemenceau S, Baulac M, Miles R. Glutamatergic pre-ictal discharges emerge at the transition to seizure in human epilepsy. *Nat Neurosci* 14: 627–634, 2011.

Jiruska P, Csicsvari J, Powell AD, Fox JE, Chang WC, Vreugdenhil M, Li X, Palus M, Bujan AF, Dearden RW, Jefferys JG. High-frequency network activity, global increase in neuronal activity, and synchrony expansion precede epileptic seizures in vitro. *J Neurosci* 30: 5690–5701, 2010.

Jouny CC, Bergey GK, Franaszczuk PJ. Partial seizures are associated with early increases in signal complexity. *Clin Neurophysiol* 121: 7–13, 2010.

Jurgens CW, Rau KE, Knudson CA, King JD, Carr PA, Porter JE, Doze VA. Beta1 adrenergic receptor-mediated enhancement of hippocampal CA3 network activity. *J Pharmacol Exp Ther* 314: 552–560, 2005.

Katsuki H, Izumi Y, Zorumski CF. Noradrenergic regulation of synaptic plasticity in the hippocampal CA1 region. *J Neurophysiol* 77: 3013–3020, 1997.

Khorkova O, Golowasch J. Neuromodulators, not activity, control coordinated expression of ionic currents. *J Neurosci* 27: 8709–8718, 2007.

Ko KH, Dailey JW, Jobe PC. Evaluation of monoaminergic receptors in the genetically epilepsy prone rat. *Experientia* 40: 70–73, 1984.

Kobayashi M, Imamura K, Sugai T, Onoda N, Yamamoto M, Komai S, Watanabe Y. Selective suppression of horizontal propagation in rat visual cortex by norepinephrine. *Eur J Neurosci* 12: 264–272, 2000.

Kong Y, Ruan L, Qian L, Liu X, Le Y. Norepinephrine promotes microglia to uptake and degrade amyloid beta peptide through upregulation of mouse formyl peptide receptor 2 and induction of insulin-degrading enzyme. *J Neurosci* 30: 11848–11857, 2010.

Krahl SE, Clark KB, Smith DC, Browning RA. Locus coeruleus lesions suppress the seizure-attenuating effects of vagus nerve stimulation. *Epilepsia* 39: 709–714, 1998.

Lands AM, Arnold A, McAuliff JP, Luduena FP, Brown TG Jr. Differentiation of receptor systems activated by sympathomimetic amines. *Nature* 214: 597–598, 1967.

Lenz RA, Pitler TA, Alger BE. High intracellular Cl- concentrations depress G-protein-modulated ionic conductances. *J Neurosci* 17: 6133–6141, 1997.

Lubenov EV, Siapas AG. Hippocampal theta oscillations are travelling waves. *Nature* 459: 534–539, 2009.

Lund C, Kostov H, Blomskjold B, Nakken KO. Efficacy and tolerability of long-term treatment with vagus nerve stimulation in adolescents and adults with refractory epilepsy and learning disabilities. *Seizure* 20: 34–37, 2011.

Madison DV, Nicoll RA. Actions of noradrenaline recorded intracellularly in rat hippocampal CA1 pyramidal neurones, in vitro. *J Physiol* 372: 221–244, 1986.

Mann EO, Tominaga T, Ichikawa M, Greenfield SA. Cholinergic modulation of the spatiotemporal pattern of hippocampal activity in vitro. *Neuropharmacology* 48: 118–133, 2005.

Mapelli J, Gandolfi D, D'Angelo E. High-pass filtering and dynamic gain regulation enhance vertical bursts transmission along the mossy fiber pathway of cerebellum. *Front Cell Neurosci* 4: 14, 2010.

McLachlan RS. Vagus nerve stimulation for intractable epilepsy: a review. *J Clin Neurophysiol* 14: 358–368, 1997.

Mennerick S, Chisari M, Shu HJ, Taylor A, Vasek M, Eisenman LN, Zorumski CF. Diverse voltage-sensitive dyes modulate $GABA_A$ receptor function. *J Neurosci* 30: 2871–2879, 2010.

Merlo D, Cifelli P, Cicconi S, Tancredi V, Avoli M. 4-Aminopyridine-induced epileptogenesis depends on activation of mitogen-activated protein kinase ERK. *J Neurochem* 89: 654–659, 2004.

Milner TA, Shah P, Pierce JP. beta-adrenergic receptors primarily are located on the dendrites of granule cells and interneurons but also are found on astrocytes and a few presynaptic profiles in the rat dentate gyrus. *Synapse* 36: 178–193, 2000.

Mody I, Lambert JD, Heinemann U. Low extracellular magnesium induces epileptiform activity and spreading depression in rat hippocampal slices. *J Neurophysiol* 57: 869–888, 1987.

Morozov A, Muzzio IA, Bourtchouladze R, Van-Strien N, Lapidus K, Yin D, Winder DG, Adams JP, Sweatt JD, Kandel ER. Rap1 couples cAMP signaling to a distinct pool of p42/44MAPK regulating excitability, synaptic plasticity, learning, and memory. *Neuron* 39: 309–325, 2003.

Mueller AL, Dunwiddie TV. Anticonvulsant and proconvulsant actions of alpha- and beta-noradrenergic agonists on epileptiform activity in rat hippocampus in vitro. *Epilepsia* 24: 57–64, 1983.

Mueller AL, Hoffer BJ, Dunwiddie TV. Noradrenergic responses in rat hippocampus: evidence for medication by alpha and beta receptors in the in vitro slice. *Brain Res* 214: 113–126, 1981.

Mueller AL, Palmer MR, Hoffer BJ, Dunwiddie TV. Hippocampal noradrenergic responses in vivo and in vitro. Characterization of alpha and beta components. *Naunyn Schmiedebergs Arch Pharmacol* 318: 259–266, 1982.

Netoff TI, Schiff SJ. Decreased neuronal synchronization during experimental seizures. *J Neurosci* 16: 7297–7307, 2002.

Oestreich EA, Wang H, Malik S, Kaproth-Joslin KA, Blaxall BC, Kelley GG, Dirksen RT, Smrcka AV. Epac-mediated activation of phospholipase C(epsilon) plays a critical role in beta-adrenergic receptor-dependent enhancement of Ca^{2+} mobilization in cardiac myocytes. *J Biol Chem* 282: 5488–5495, 2007.

Pedarzani P, Storm JF. Interaction between alpha- and beta-adrenergic receptor agonists modulating the slow Ca^{2+}-activated K^+ current I_{AHP} in hippocampal neurons. *Eur J Neurosci* 8: 2098–2110, 1996.

Pena F, Ramirez JM. Substance P-mediated modulation of pacemaker properties in the mammalian respiratory network. *J Neurosci* 24: 7549–7556, 2004.

Perreault P, Avoli M. Physiology and pharmacology of epileptiform activity induced by 4-aminopyridine in rat hippocampal slices. *J Neurophysiol* 65: 771–785, 1991.

Pinto DJ, Patrick SL, Huang WC, Connors BW. Initiation, propagation, and termination of epileptiform activity in rodent neocortex in vitro involve distinct mechanisms. *J Neurosci* 25: 8131–8140, 2005.

Prida LM, Sanchez-Andres JV. Nonlinear frequency-dependent synchronization in the developing hippocampus. *J Neurophysiol* 82: 202–208, 1999.

Puig MV, Watakabe A, Ushimaru M, Yamamori T, Kawaguchi Y. Serotonin modulates fast-spiking interneuron and synchronous activity in the rat prefrontal cortex through $5\text{-}HT_{1A}$ and $5\text{-}HT_{2A}$ receptors. *J Neurosci* 30: 2211–2222, 2010.

Raiesdana S, Golpayegani SM, Firoozabadi SM, Mehvari Habibabadi J. On the discrimination of patho-physiological states in epilepsy by means of dynamical measures. *Comput Biol Med* 39: 1073–1082, 2009.

Reddy DS. Neurosteroids: endogenous role in the human brain and therapeutic potentials. *Prog Brain Res* 186: 113–137, 2010.

Roosevelt RW, Smith DC, Clough RW, Jensen RA, Browning RA. Increased extracellular concentrations of norepinephrine in cortex and hippocampus following vagus nerve stimulation in the rat. *Brain Res* 1119: 124–132, 2006.

Rutecki PA. Noradrenergic modulation of epileptiform activity in the hippocampus. *Epilepsy Res* 20: 125–136, 1995.

Sanchez-Vives MV, McCormick DA. Cellular and network mechanisms of rhythmic recurrent activity in neocortex. *Nat Neurosci* 3: 1027–1034, 2000.

Schiff S, Cressman JR, Barreto E, Žiburkus J. Towards a dynamics of seizure mechanics. In: *Computational Neuroscience in Epilepsy*, edited by Soltesz I. London: Elsevier Academic, 2008, p. 496–514.

Seol GH, Žiburkus J, Huang S, Song L, Kim IT, Takamiya K, Huganir RL, Lee HK, Kirkwood A. Neuromodulators control the polarity of spike-timing-dependent synaptic plasticity. *Neuron* 55: 919–929, 2007.

Sinha SR, Saggau P. Imaging of 4-AP-induced, $GABA_A$-dependent spontaneous synchronized activity mediated by the hippocampal interneuron network. *J Neurophysiol* 86: 381–391, 2001.

Storm JF. Action potential repolarization and a fast after-hyperpolarization in rat hippocampal pyramidal cells. *J Physiol* 385: 733–759, 1987.

Svensson E, Grillner S, Parker D. Gating and braking of short- and long-term modulatory effects by interactions between colocalized neuromodulators. *J Neurosci* 21: 5984–5992, 2001.

Szot P, Weinshenker D, Rho JM, Storey TW, Schwartzkroin PA. Norepinephrine is required for the anticonvulsant effect of the ketogenic diet. *Brain Res Dev Brain Res* 129: 211–214, 2001.

Szot P, Weinshenker D, White SS, Robbins CA, Rust NC, Schwartzkroin PA, Palmiter RD. Norepinephrine-deficient mice have increased susceptibility to seizure-inducing stimuli. *J Neurosci* 19: 10985–10992, 1999.

Tang LQ, Hong PH, Siddiqui Y, Sarkissian ES, Huang RY, Lee E, Krupin T. Effect of beta-adrenergic agents on intracellular potential of rabbit ciliary epithelium. *Curr Eye Res* 17: 24–30, 1998.

Thompson S. Aminopyridine block of transient potassium current. *J Gen Physiol* 80: 1–18, 1982.

Tominaga T, Tominaga Y. $GABA_A$ receptor-mediated modulation of neuronal activity propagation upon tetanic stimulation in rat hippocampal slices. *Pflügers Arch* 460: 875–889, 2010.

Tominaga T, Tominaga Y, Yamada H, Matsumoto G, Ichikawa M. Quantification of optical signals with electrophysiological signals in neural activities of Di-4-ANEPPS stained rat hippocampal slices. *J Neurosci Methods* 102: 11–23, 2000.

Traub RD, Borck C, Colling SB, Jefferys JG. On the structure of ictal events in vitro. *Epilepsia* 37: 879–891, 1996.

Traub RD, Colling SB, Jefferys JG. Cellular mechanisms of 4-aminopyridine-induced synchronized after-discharges in the rat hippocampal slice. *J Physiol* 489: 127–140, 1995.

Traub RD, Jefferys JG, Whittington MA. Enhanced NMDA conductance can account for epileptiform activity induced by low Mg^{2+} in the rat hippocampal slice. *J Physiol* 478: 379–393, 1994.

Uhlhaas PJ, Pipa G, Lima B, Melloni L, Neuenschwander S, Nikolic D, Singer W. Neural synchrony in cortical networks: history, concept and current status. *Front Integr Neurosci* 3: 17, 2009.

Ul Haq R, Liotta A, Kovacs R, Rosler A, Jarosch MJ, Heinemann U, Behrens CJ. Adrenergic modulation of sharp wave-ripple activity in rat hippocampal slices. *Hippocampus* 22: 516–533, 2012.

Vale FL, Ahmadian A, Youssef AS, Tatum WO, Benbadis SR. Long-term outcome of vagus nerve stimulation therapy after failed epilepsy surgery. *Seizure* 20: 244–248, 2011.

Van Vreeswijk C, Abbott LF, Ermentrout GB. When inhibition not excitation synchronizes neural firing. *J Comput Neurosci* 1: 313–321, 1994.

Vaughan CW, Christie MJ. Retrograde signalling by endocannabinoids. *Handb Exp Pharmacol* 367–383, 2005.

Wahab A, Albus K, Gabriel S, Heinemann U. In search of models of pharmacoresistant epilepsy. *Epilepsia* 51, Suppl 3: 154–159, 2010.

Weinshenker D, Szot P. The role of catecholamines in seizure susceptibility: new results using genetically engineered mice. *Pharmacol Ther* 94: 213–233, 2002.

Weinshenker D, Szot P, Miller NS, Palmiter RD. Alpha(1) and beta(2) adrenoreceptor agonists inhibit pentylenetetrazole-induced seizures in mice lacking norepinephrine. *J Pharmacol Exp Ther* 298: 1042–1048, 2001.

Weissinger F, Buchheim K, Siegmund H, Meierkord H. Seizure spread through the life cycle: optical imaging in combined brain slices from immature, adult, and senile rats in vitro. *Neurobiol Dis* 19: 84–95, 2005.

Wu JY, Xiaoying H, Chuan Z. Propagating waves of activity in the neocortex: what they are, what they do. *Neuroscientist* 14: 487–502, 2008.

Zecevic D, Djurisic M, Cohen LB, Antic S, Wachowiak M, Falk CX, Zochowski MR. Imaging nervous system activity with voltage-sensitive dyes. *Curr Protoc Neurosci* 6: 6–17, 2003.

Zhong H, Minneman KP. Alpha1-adrenoceptor subtypes. *Eur J Pharmacol* 375: 261–276, 1999.

Žiburkus J, Cressman JR, Barreto E, Schiff SJ. Interneuron and pyramidal cell interplay during in vitro seizure-like events. *J Neurophysiol* 95: 3948–3954, 2006.

Zsiros V, Maccaferri G. Noradrenergic modulation of electrical coupling in GABAergic networks of the hippocampus. *J Neurosci* 28: 1804–1815, 2008.